

The role of symmetries in adiabatic quantum algorithms

Gernot Schaller¹ and Ralf Schützhold²

*1 Institut für Theoretische Physik, Hardenbergstraße 36,
Technische Universität Berlin, D-10623 Berlin, Germany*

*2 Institut für Theoretische Physik, Lotharstraße 1,
Universität Duisburg-Essen, D-47048 Duisburg, Germany*

Exploiting the similarity between adiabatic quantum algorithms and quantum phase transitions, we argue that second-order transitions – typically associated with broken or restored symmetries – should be advantageous in comparison to first-order transitions. Guided by simple examples we construct an alternative adiabatic algorithm for the NP-complete problem *Exact Cover 3*. We show numerically that its average performance (for the considered cases up to $\mathcal{O}\{20\}$ qubits) is better than that of the conventional scheme. The run-time of adiabatic algorithms is not just determined by the minimum value of the fundamental energy gap (between the ground state and the excited states), but also by its curvature at the critical point. The proposed symmetry-restoring adiabatic quantum algorithm only contains contributions linear and quadratic in the Pauli matrices and can be generalized to other problem Hamiltonians which are decomposed of terms involving one and two qubits. We show how the factoring problem can be cast into such a quadratic form. These findings suggest that adiabatic quantum algorithms can solve a large class of NP problems much faster than the Grover search routine (which corresponds to a first-order transition and yields a quadratic enhancement only).

PACS numbers: 03.67.-a, 03.67.Lx, 73.43.Nq.

I. INTRODUCTION

A. Adiabatic quantum algorithms

The overwhelming potential of quantum computers in number factorization [1] and database search [2] has initiated a lot of research. In the conventional (sequential) quantum algorithmic approach, unitary single and two-qubit operations are applied on a quantum state and the result of the computation can then be extracted (probabilistically) by measurement. Unfortunately, the promises of quantum computing are strongly hampered by the devastating influence of decoherence: Inevitable couplings with the reservoir tend to destroy the fragile quantum coherence. The available error correction schemes require further auxiliary qubits [3] and – although even strongly correlated errors can in principle be corrected [4] – become increasingly complex with admitting more and more general errors.

Farhi *et al.* have proposed an alternative scheme with an inherent error protection: adiabatic quantum computation [5, 6]. In this scheme, the solution to a problem is encoded as the (unknown) ground state of a (known) problem Hamiltonian H_F , which is separated by a sufficiently large energy gap from excited states. Computation will start with a different initial Hamiltonian H_I possessing a known and easily preparable ground state, which is also well separated energetically from all other states. The system is prepared in this ground state and then the initial Hamiltonian H_I is continuously deformed into the final problem Hamiltonian H_F . The adiabatic theorem guarantees that if the evolution is slow enough, the system will stay near its instantaneous eigenstate and will thus finally reach the ground state of the prob-

lem Hamiltonian [8]. Thus, the solution to the problem can be extracted by measurement of the final quantum state. A nice advantage of this quantum computation scheme (which is believed to be polynomially equivalent to sequential quantum computation [7]) lies in the robustness of the ground state against the influences of decoherence – a sufficiently cold reservoir provided [9, 10, 11, 12, 13, 14, 15, 16, 17, 18]: The ground state cannot decay and phase errors do not play any role, i.e., errors can only result from excitations. The speed (total evolution time T) at which the interpolation between the two Hamiltonians can be performed without strongly exciting higher eigenstates of the system is related to the inverse gap between the instantaneous lowest and first excited eigenvalues [8]. The total evolution time T required to reach a fixed fidelity in the final state can be interpreted as the algorithmic complexity of the adiabatic computation scheme. With using a constant deformation speed (ignoring the structure of the fundamental energy gap) the adiabatic run-time will scale as $T = \mathcal{O}\{g_{\min}^{-2}\}$, whereas with knowledge on the fundamental gap this can under fairly moderate assumptions even be improved to $T = \mathcal{O}\{g_{\min}^{-1}\}$ [19, 20].

This also highlights the main obstacle in adiabatic quantum computation: Typically, the minimum fundamental gap g_{\min} decreases strongly with increasing system size (number of qubits) for nontrivial problems. For example, in the adiabatic version of Grover's algorithm [21], the minimum fundamental gap decreases exponentially $g_{\min} = 2^{-n/2}$ with system size n . An analogous exponential scaling of the minimum fundamental gap has been found in other adiabatic quantum algorithms with similar initial Hamiltonians [22]. However, it has been argued that this exponential scaling is a result of the un-

favorable choice of the initial Hamiltonian and can be avoided for more suitable choices [23]. In these cases, however, g_{\min} is not known analytically. Numerical analysis in [5, 6] seems to indicate a quadratic scaling $T \sim n^2$ of the algorithmic complexity with the system size n – but this favorable scaling could perhaps be just a consequence of choosing particularly simple problems, cf. [24, 25]. Therefore, the speed-up attainable with these adiabatic quantum algorithms is still an open question.

B. Quantum phase transitions

As has been noted earlier [26, 27], adiabatic quantum algorithms display a remarkable similarity with sweeps through quantum phase transitions: During the adiabatic interpolation, the ground state changes from the simple initial ground state of H_I to the unknown solution of some problem encoded in H_F . Typically, on the way from H_I to H_F , one encounters a critical point where the fundamental gap (which is sufficiently large initially and finally) becomes very small. Near the position of the minimum gap, the ground state will change more drastically than during other time intervals of the interpolation

$$\|\dot{\psi}_0\|^2 \equiv \langle \dot{\psi}_0 | \dot{\psi}_0 \rangle \geq \sum_{n>0} \left| \frac{\langle \dot{\psi}_0 | \dot{H} | \psi_n \rangle}{E_n - E_0} \right|^2, \quad (1)$$

where we have inserted an identity and expressed $\langle \dot{\psi}_0 | \dot{\psi}_n \rangle$ by the time-derivative of the eigenvalue equation $H(t)|\psi_0(t)\rangle = E_0(t)|\psi_0(t)\rangle$. If the relevant fundamental energy gap (the smallest one with $\langle \dot{\psi}_0 | \dot{H} | \psi_n \rangle \neq 0$) scales inversely with the system size, we see directly that in the infinite-size limit, the ground state will change non-analytically at the critical point. This singularity would completely prohibit an adiabatic evolution in this limit. However, for practical problems one is interested in the finite-size scaling of an algorithm, where it makes a huge difference whether its computational complexity increases *exponentially* or merely *polynomially* with the system size n . The same principle applies to the efficient suppression of thermal excitations when the quantum system is coupled to a low-temperature bath [9], where it may prove experimentally difficult to apply polynomially small temperatures and most likely infeasible to apply exponentially small temperatures.

In the following, we shall exploit the analogy between adiabatic quantum algorithms and quantum phase transitions further in order to gain additional insight into these issues. Beyond the behaviour of the minimum gap, the complexity of implementing the involved Hamiltonians (number of interactions between different qubits) is of experimental importance and shall also be addressed.

II. MOTIVATION

A. Grover Search Routine

The adiabatic version of Grover's search algorithm is defined by the linear interpolation $H(s) = (1-s)H_I + sH_F$, where $s \in [0, 1]$ between the Hamiltonians [21]

$$H_I = \mathbf{1} - |S\rangle\langle S|, \quad H_F = \mathbf{1} - |w\rangle\langle w|, \quad (2)$$

where the initial ground state

$$|S\rangle = \frac{1}{\sqrt{N}} \sum_{z=0}^{N-1} |z\rangle = |\rightarrow\rangle \otimes \dots \otimes |\rightarrow\rangle \quad (3)$$

is the superposition vector of all $N = 2^n$ states in the computational (σ_z) basis and $|\rightarrow\rangle = (|0\rangle + |1\rangle)/\sqrt{2} = (|\downarrow\rangle + |\uparrow\rangle)/\sqrt{2}$. In contrast, the final ground state $|w\rangle$ is some distinguished computational basis state.

It is straightforward to derive the instantaneous spectrum of $H(s)$ by Erhard-Schmidt orthogonalization, for example. One obtains the fundamental gap

$$g(s) = \sqrt{1 - 4 \left(1 - \frac{1}{2^n}\right) s(1-s)}, \quad (4)$$

and the two non-trivial levels $E_{0/1}(s) = \frac{1}{2}[1 \pm g(s)]$ as well as $E_2(s) = \dots = E_{N-1}(s) = 1$. Thus, the adiabatic Grover algorithm continuously transforms the initial vacuum $|S\rangle$ towards the final ground state $|w\rangle$, see also figure 1. From Equation (4) we may infer an exponentially

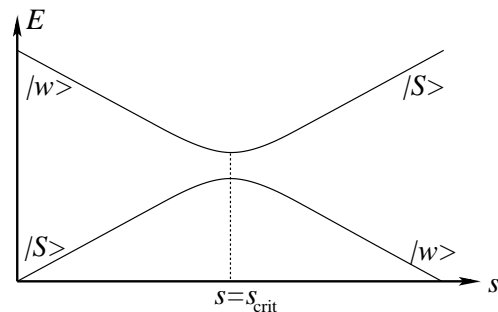


FIG. 1: Sketch of the two lowest energy levels for the Grover problem as a prototypical example for a first-order quantum phase transition in the infinite size limit $n \uparrow \infty$ (where the energy gap vanishes and the avoided level crossing becomes a real crossing).

small minimum fundamental gap $g_{\min} = \sqrt{1/2^n}$ at the critical point $s_{\text{crit}} = 1/2$.

In the infinite-size limit ($n \rightarrow \infty$), the first derivative dE_0/ds of the ground state energy $E_0(s)$ jumps at the point of the phase transition $s_{\text{crit}} = 1/2$. In view of the equality

$$\frac{dE_0(s)}{ds} = \left\langle \psi_0(s) \left| \frac{dH(s)}{ds} \right| \psi_0(s) \right\rangle, \quad (5)$$

this discontinuity goes along with a jump in certain expectation values (e.g., $\langle dH/ds \rangle$) and hence order parameters such as the horizontal magnetization $\langle \sigma_x \rangle$ change abruptly at the critical point $s_{\text{crit}} = 1/2$. Conventionally, this property (discontinuous order parameter) is used to classify the phase transition as a first-order transition.

From Eqn. (1) it follows that the ground state basically jumps from $|\psi_0(s < 1/2)\rangle = |S\rangle$ to $|\psi_0(s > 1/2)\rangle = |w\rangle$. Such an abrupt change is a general feature of first-order quantum phase transitions and can be understood in terms of a time-dependent energy landscape. Assuming a separable state (compare also [28, 29] for a similar approach)

$$|\varphi\rangle = \bigotimes_{i=1}^n [\cos(\varphi) |0\rangle + \sin(\varphi) |1\rangle]_i \quad (6)$$

and re-ordering the states in the computational basis such that $|w\rangle = |1\dots 1\rangle$ (the initial state (3) is invariant to this transformation) we can calculate the semiclassical energy landscape

$$\begin{aligned} E(s, \varphi) &\equiv \langle \varphi | H(s) | \varphi \rangle \\ &= 1 - (1-s) \frac{[\cos(\varphi) + \sin(\varphi)]^{2n}}{2^n} \\ &\quad - s \sin^n(\varphi), \end{aligned} \quad (7)$$

shown in Fig. 2. We see that even in this semiclassical

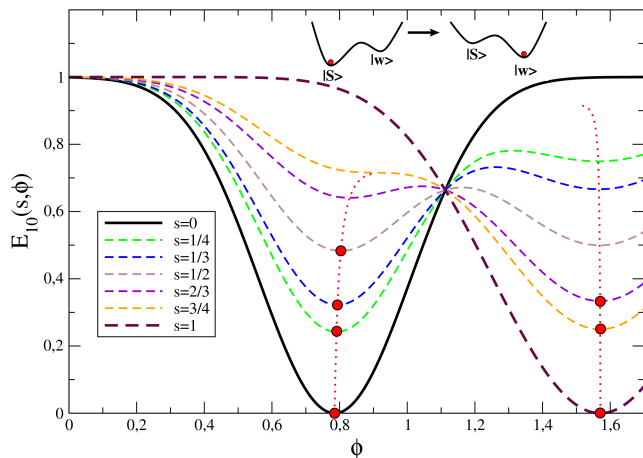


FIG. 2: Semiclassical energy landscapes (7) for the Grover problem with $n = 10$ spins for different interpolation parameters s . In order to stay in the global minimum, the system has to tunnel through an energy barrier that does not vanish throughout the interpolation, i.e., the time-dependent position (red dotted lines) of the two local minima is not connected. Circle symbols show the position of the global minimum.

picture the two minima are always separated – either by a potential barrier or by large energy differences. This corresponds to the existence of a tunneling barrier between the two minima.

The time-dependent Hamiltonian (2) does not have a conserved quantity, such that the initial ground state $|S\rangle$ does not break any symmetry of the initial Hamiltonian. We conjecture that in the absence of additional conserved quantities (related to continuous symmetries of the Hamiltonian), there are always two (or more) competing local minima whose energies depend on the interpolation parameter s . At the critical point s_{crit} , the order of the s -dependent energy minima changes and thus the global minimum makes a jump. Consequently, in order to stay in the true ground state, the quantum system has to tunnel through the barrier depicted in figure 2. Since one would naturally expect that all the energy scales and hence also the size of the tunneling barrier increase roughly linearly with system size n , the tunneling probability decreases exponentially with the number of qubits n . This intuitive picture suggests that the runtime T needed to stay in the ground state scales exponentially for all first-order transitions. Indeed, since the tunneling amplitude provides the coupling between the competing ground states and hence determines the minimum gap g_{min} in their avoided level crossing, such an exponential scaling is precisely what one finds for the adiabatic Grover algorithm and further adiabatic algorithms [22, 23, 25] with similar initial Hamiltonian – which all correspond to first-order transitions.

B. Transverse Ising model

After having discussed first-order transitions, let us turn to a prototypical model for a second-order quantum phase transition [30]. The one-dimensional transverse Ising model is given by linear interpolation between

$$H_I = - \sum_{\ell=1}^n \sigma_{\ell}^x, \quad H_F = - \sum_{\ell=1}^n \sigma_{\ell}^z \sigma_{\ell+1}^z, \quad (8)$$

where $\sigma_{\ell}^{x/y}$ denote the Pauli spin matrices acting on the ℓ^{th} qubit and periodic boundary conditions $\sigma_{n+1}^z = \sigma_1^z$ are assumed. At any point during the interpolation, the Hamiltonian $H(s)$ can be diagonalized analytically: The successive application of Jordan-Wigner, Fourier, and Bogoliubov transformations [30] map the interacting spin-1/2-Hamiltonian (8) to a set of non-interacting fermionic quasi-particles

$$H = \sum_k \epsilon_k \left(\gamma_k^{\dagger} \gamma_k - \frac{1}{2} \right), \quad (9)$$

with fermionic creation and annihilation operators $\gamma_k^{\dagger}, \gamma_k$ and single quasi-particle energies

$$\epsilon_k(s) = 2\sqrt{1 - 4 \cos^2(ka/2) s(1-s)}, \quad (10)$$

see figure 3. The wavenumber ka covers the range $ka = (1 + 2\mathbb{Z})\pi/n \quad : \quad |ka| < \pi$. Both Hamiltonians in

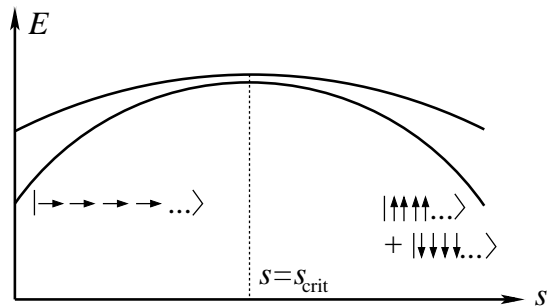


FIG. 3: Sketch of the two lowest energy eigenvalues for the Ising model as a prototypical example of a second-order quantum phase transition. In contrast to figure 1, the geometry near the minimum gap does not correspond to an isolated avoided crossing.

(8) obey a 180-degree rotational symmetry around the σ_ℓ^x -axes (bit-flip)

$$\left[H_I, \bigotimes_{\ell=1}^n \sigma_\ell^x \right] = \left[H_F, \bigotimes_{\ell=1}^n \sigma_\ell^x \right] = 0 \quad (11)$$

which transforms σ_i^z to $-\sigma_i^z$. Since due to Eqn. (11) the even bit-flip parity of the unique initial ground state $|S\rangle$ is a conserved quantity, the symmetry of the two-fold degenerate final ground state $|\Psi_0^1\rangle = |\uparrow \dots \uparrow\rangle$ and $|\Psi_0^2\rangle = |\downarrow \dots \downarrow\rangle$ is broken, such that for adiabatic evolution, the system will end up in the macroscopic superpositions (Schrödinger's cat) state

$$|\Psi_0^{\text{even}}\rangle = \frac{|\uparrow \dots \uparrow\rangle + |\downarrow \dots \downarrow\rangle}{\sqrt{2}}. \quad (12)$$

The minimum gap can be obtained from equation (10) and scales polynomially $g_{\text{min}} = \mathcal{O}\{1/n\}$. Therefore, the adiabatic runtime T does also scale polynomially – a constant speed interpolation, for example, yields $T_{\text{ad}} = \mathcal{O}\{n^2\}$ [31]. Furthermore, since the wavenumber ka covers the range $ka = (1 + 2\mathbb{Z})\pi/n$: $|ka| < \pi$, the infinite-size limit of the ground state energy can be obtained by replacing the sum over the single-particle energies by an integral

$$E_0^{\text{cont}}(s) = - \lim_{n \rightarrow \infty} \sum_{ka} \frac{\epsilon_k}{2} = -\frac{2n}{\pi} \mathcal{E} \left(2\sqrt{s(1-s)} \right), \quad (13)$$

where $\mathcal{E}(x)$ denotes the complete elliptic integral. In contrast to the previous subsection II A, the energy density $\mathcal{E}(1) = 1$ and its first derivative $\mathcal{E}'(1) = 0$ are well defined at the critical point. Since $\langle H(s) \rangle$ and $\langle dH/ds \rangle$ are continuous across the transition, there is no jump in order parameters such as $\langle \sigma_x \rangle$ and the ground state changes less abruptly. However, the second derivative of the ground state energy diverges at the critical point $\mathcal{E}''(1) = \infty$ and hence, we classify the Ising model as a second order quantum phase transition, compare also [30]. Consequently, we have a symmetry-breaking quantum phase transition of second order.

As in the previous section, we can derive a semiclassical time-dependent energy landscape with the separable ansatz (6) to obtain

$$E_n(s, \varphi) = n \left\{ - (1-s) \sin(2\varphi) - s [\cos^2(\varphi) - \sin^2(\varphi)]^2 \right\}, \quad (14)$$

where the bit-flip invariance (11) is reflected by a mirror symmetry of the energy landscape around $\varphi = \pi/4$, see figure 4. We see that symmetry-breaking/restoring quan-

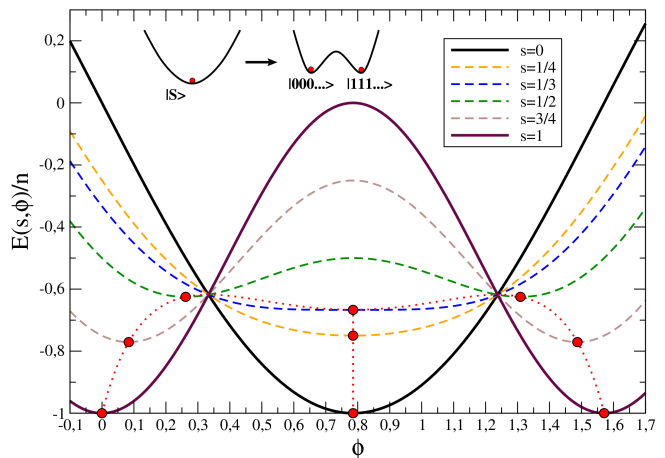


FIG. 4: Semiclassical energy density landscape for the Ising model in a transverse field for different interpolation parameters s . In contrast to first-order transitions, there is no energy barrier between the initial and the final ground state, i.e., the time-dependent positions (red dotted line) of the minima are always connected.

tum phase transitions are typically of second (or higher) order, i.e., the ground state does not change as abruptly as in first-order transitions. Consequently, the system does not need to tunnel through a barrier in order to stay in the global vacuum. As a result, the reason for the exponential scaling of the run-time T we found for first-order transitions is absent in the case of quantum phase transitions of second or higher order, which is consistent with the polynomial scaling of gap [30] and adiabatic runtime [31].

Evidently, the transverse Ising model can also be considered an adiabatic quantum algorithm, although of course the final ground states are trivial – the problem to be solved is simply “How can all bits have the same value?” Note that, reversing the evolution and slowly interpolating from H_F towards H_I in (8), the final state will be close to the true unique ground state $|S\rangle$ if and only if initialized with the superposition (12).

C. Mixed Case

Even though the concept of broken or restored symmetries is very useful for classifying quantum phase

transitions, it should be stressed that symmetry breaking/restoration alone does not guarantee a second-order transition. As an intuitive counterexample, one may consider the linear interpolation between

$$H_I = \mathbf{1} - |S\rangle\langle S|, \quad H_F = \sum_{\ell=1}^n \frac{1}{2} [1 - \sigma_{\ell}^z \sigma_{\ell+1}^z], \quad (15)$$

which has an equivalent (up to shifting and scaling to obtain positive definiteness) final Hamiltonian as (8) but differs in the initial Hamiltonian, for which we have chosen the initial Hamiltonian of the Grover problem (2). Evidently, the ground state symmetry of the final Hamiltonian is also broken, since the bit-flip parity is also conserved. However, an analysis of the semiclassical energy landscapes generated with a separable ansatz (6) yields

$$E_n(s, \varphi) = (1-s) \left\{ 1 - \frac{[\cos(\varphi) + \sin(\varphi)]^{2n}}{2^n} \right\} + \frac{ns}{2} \left\{ 1 - [\cos^2(\varphi) - \sin^2(\varphi)]^2 \right\}, \quad (16)$$

which also exhibits a mirror symmetry at $\varphi = \pi/4$ but always has a tunneling barrier between the vacua, see figure 5. The level structure displays the geometry of an

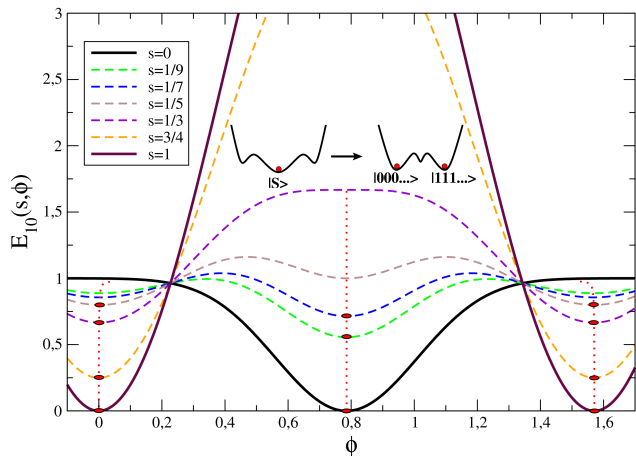


FIG. 5: Semiclassical energy landscapes for a symmetry-breaking quantum phase transition – which is, however, not of second but of first order. In spite of the symmetry breaking, there is a tunneling barrier throughout the interpolation and a jump between the initial and the final ground state(s), i.e., the position of the vacua (dotted red lines) is not connected.

avoided level crossing at the critical point, i.e., it corresponds to a first-order phase transition, see Figure 6. In accordance with our previous arguments, it can be shown analytically that the gap scales exponentially in such a situation [22, 23, 25].

In order to understand why the phase transition is of first order, it might be useful to recall that the initial Hamiltonian is a projector that involves n -qubit interac-

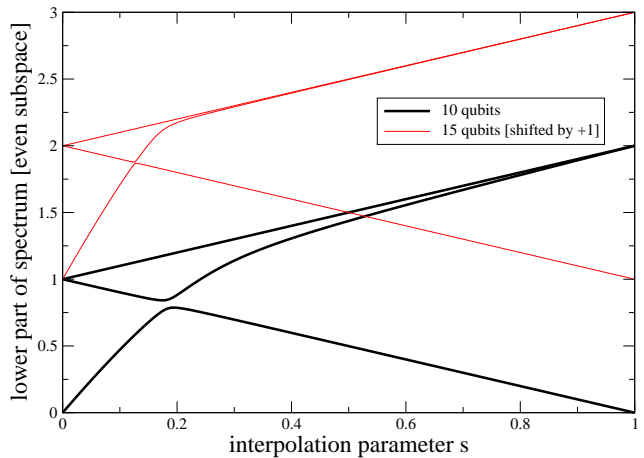


FIG. 6: Lowest eigenvalues of the Hamiltonian (15) for 10 (bold black lines) and 15 (thin red lines, shifted for better readability) qubits in the relevant subspace which is even under bit-flip. One can clearly see that the spectrum displays an avoided level crossing at the critical point – thus corresponding to a first-order transition.

tions

$$H_I = \mathbf{1} - |S\rangle\langle S| = \mathbf{1} - \bigotimes_{\ell=1}^n \frac{\mathbf{1} + \sigma_{\ell}^x}{2}. \quad (17)$$

The bit structures of the initial and the final Hamiltonian are very different and, in this sense, their “distance” in the space of all matrices is very large.

D. Conjecture

We have seen for the Grover example that first order quantum phase transitions are associated with an exponential scaling of the adiabatic runtime with the system size n . For local Hamiltonians, this observation can be generalized [33]: For a typical first order transition one has two locally distinguishable competing ground states $|\tilde{w}\rangle$ and $|\tilde{s}\rangle$ that exchange their energetic favorability right at the critical point $\langle \tilde{w} | H | \tilde{w} \rangle|_{s_{\text{crit}}} = \langle \tilde{s} | H | \tilde{s} \rangle|_{s_{\text{crit}}}$. Their overlap is exponentially small (due to local distinguishability) and for a local reasonable (with polynomial matrix elements) Hamiltonian this also implies that $\langle \tilde{s} | H | \tilde{w} \rangle \propto \exp\{-\mathcal{O}(n)\}$ is also exponentially small. In the two-dimensional subspace spanned by these states the energy gap equates to $g_{\text{crit}} = 2|\langle \tilde{s} | H | \tilde{w} \rangle|$, which becomes therefore exponentially small.

Our conjecture is therefore that for adiabatic quantum algorithms

- higher order quantum phase transitions are more advantageous than first order quantum phase transitions and
- such higher order transitions might be induced by interpolations respecting a conserved quantity (leading to spontaneous symmetry breaking in the degenerate

ground state of one Hamiltonian) in combination with similar bit structures in initial and final Hamiltonians.

Of course, these considerations are very intuitive and by no means conclusive – but they will hopefully help us to design more powerful quantum algorithms. For example, it would of course be nice to have no phase transition at all (which corresponds to a constant lower bound on the fundamental energy gap [32]) but numerous numerical [24, 26, 27, 34, 35] and analytical [22, 25] evidence suggests that this is not the case for hard optimization problems.

III. RUNTIME SCALING FOR LINEAR QUENCHING

The main measure for the computational complexity of adiabatic quantum algorithms is the minimum runtime T . In the following, we derive an estimate of the runtime T based on the level structure of the adiabatic quantum algorithm. We will assume a linear quench $s = t/T$ and a single isolated position of the minimum energy gap. In cases where the position and size of this minimum energy gap is explicitly known, one can improve the runtime by adapting the interpolation speed (i.e., moving fast away from the critical point and slow in its vicinity) [19, 21]. However, since the exact position of the minimum gap is not known *a priori* for most of the interesting cases – although its approximate position can be estimated by perturbative and other (such as e.g., Gershgorin’s circle theorem) methods [7] – we shall work with a constant-speed interpolation.

As derived in [19], the final occupation amplitude of the first excited state $a_1(s = 1)$ can be obtained formally from the adiabatic expansion *via*

$$a_1(1)e^{-i\gamma_1(1)} = - \int_0^1 ds a_0(s) e^{-i\gamma_1(s)} \frac{F_{01}(s)}{g(s)} \times \exp \left\{ -iT \int_0^s g(s') ds' \right\}, \quad (18)$$

where $F_{01}(s)$ denotes the transition matrix element of $H'(s)$ in the instantaneous energy basis, $a_0(s)$ the ground-state amplitude, and γ_1 is a pure phase (including the Berry phase). The ds -integration along the real axis in the above integral can be deformed in the lower complex half-plane [19], where it is visible that for slow interpolations (large T), the outer integrand in (18) is exponentially suppressed (adiabatic approximation). However, such a deformation will be limited by singularities of $g^{-1}(s)$ at \tilde{s} located in the complex plane near the minimum of $g(s)$ on the real axis. This determines how the adiabatic runtime T has to scale with the spectral properties in order to suppress the excitation amplitude in

(18) efficiently

$$\Re \left[iT \int_0^{\Re(\tilde{s}) + i\Im(\tilde{s})/2} g(s) ds \right] \gg 1, \quad (19)$$

for a detailed discussion see [19]. Assuming a sufficiently smooth behavior, we Taylor-Laurent expand the fundamental gap near its minimum (which is a saddle-point in the complex plane)

$$g(s) \approx g_{\min} + c_{\min} (s - s_{\text{crit}})^2, \quad (20)$$

where g_{\min} denotes the value and c_{\min} the curvature of the fundamental gap at the critical point $s = s_{\text{crit}}$. The singularities of $1/g(s)$ are then found at approximately $\tilde{s} \approx s_{\text{crit}} \pm i\sqrt{g_{\min}/c_{\min}}$, which yields for the left hand side of (19)

$$\Re \left[iT \int_0^{s_{\text{crit}} - i\sqrt{g_{\min}/c_{\min}}/2} g(s) ds \right] = \mathcal{O} \left\{ T \frac{g_{\min}^{3/2}}{c_{\min}^{1/2}} \right\}. \quad (21)$$

Consequently, the runtime necessary to suppress the excitation amplitude (18) efficiently scales as

$$T = \mathcal{O} \left\{ \sqrt{\frac{c_{\min}}{g_{\min}^3}} \right\}. \quad (22)$$

Evidently, the runtime does not only depend on the value of the minimum gap g_{\min} but also on its curvature c_{\min} at the critical point $s = s_{\text{crit}}$. At first sight, this may seem counterintuitive, since from a naive interpretation of the adiabatic theorem (focusing on the minimum gap only), one would expect that a small curvature (which implies a longer persistence of a small gap) should lead to longer run-times. However, it should be kept in mind that a large curvature means a rapid change of the spectral characteristics of the Hamiltonian and hence the system will find it harder to follow the evolution in order to stay in the ground state [19, 20].

As a consistency check, we show that (22) correctly reproduces the scaling of the adiabatic runtime found earlier for the Grover problem and the Ising model in case of constant-speed interpolation: For the Grover model, one obtains from equation (4)

$$T \sim \sqrt{\frac{g_G''(s_{\text{crit}})}{g_G^3(s_{\text{crit}})}} = 2N - 1 + \mathcal{O} \left\{ \frac{1}{N} \right\}, \quad (23)$$

which implies an exponential scaling of the adiabatic runtime (since $N = 2^n$) with the system size, compare also [19, 21] and subsection II A. Likewise, one obtains for the Ising model from equation (10)

$$T \sim \sqrt{\frac{g_I''(s_{\text{crit}})}{g_I^3(s_{\text{crit}})}} = \frac{2}{\pi^2} n^2 - \frac{1}{12} + \mathcal{O} \left\{ \frac{1}{n} \right\} \quad (24)$$

a quadratic scaling of the adiabatic runtime, see also [31] and subsection II B.

We have numerically calculated the curvature and value of the minimum gap for interesting adiabatic optimization problems (see the following subsections) and have then related the adiabatic runtime T with its estimator $\sqrt{c_{\min}/g_{\min}^3}$. Our numerical experiments also confirm this scaling law quite nicely, see figure 7.

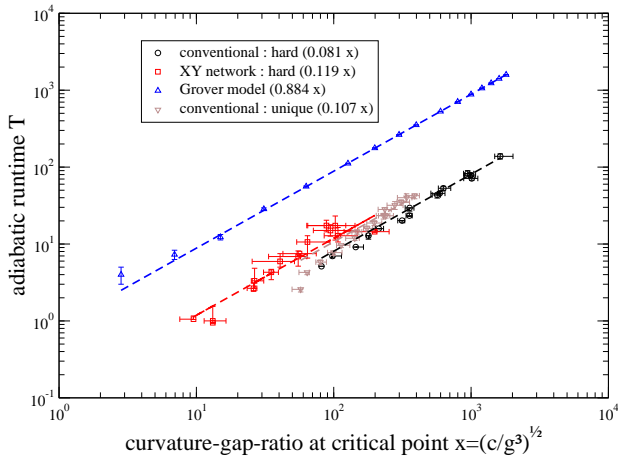


FIG. 7: [Color Online] Scaling of the adiabatic runtime from figure 8 versus $\sqrt{c_{\min}/g_{\min}^3}$ for different adiabatic algorithms. All data sets agree nicely with the relation (dashed fit lines) predicted by equation (22). With the exception of the Grover algorithm, each symbol corresponds to the median of 100 random instances with a unique satisfying agreement without constraints (brown) on the number of clauses or with $m \leq 2/3n$ clauses (black and red). Values for the linear fits (dashed lines) are given in brackets. Horizontal error bars give the 99% confidence interval on the median, whereas vertical error bars result from the finite precision when determining the necessary runtime by repeated integration of the Schrödinger equation. The data sets for Grover interpolation stem from [19], where a different success probability of $P_{\text{final}}^G = 0.75$ had been demanded.

IV. QUADRATIC SPIN HAMILTONIANS

Our conjecture (subsection II D) can be exploited to improve the search for ground states of quite general quadratic Hamiltonians. It is well known that the ground state of a frustrated anti-ferromagnet under the influence of a local field as described by the Hamiltonian

$$H_F = \sum_{i=1}^n f_i \sigma_i^z + \sum_{i,j=1}^n f_{ij} \sigma_i^z \sigma_j^z \quad (25)$$

is in general extremely (NP-)hard to find [46]. In above equation, the coefficients f_i and $f_{ij} = f_{ji}$ (with $f_{ii} = 0$) denote the local field and the interaction topology, respectively. More technically speaking, deciding whether the minimum energy of (25) lies below a certain threshold belongs to the class NP, i.e., it can be verified for

a given solution with polynomial effort – whereas actually finding the solution can be much (e.g., exponentially) harder. For Exact Cover 3, this decision problem is even NP-complete [5], which implies that all other problems in NP (i.e., decision versions of factoring, traveling salesmen problem, etc.) can be mapped to it with using only polynomial overhead. There is no classical algorithm known that delivers a solution using only polynomial resources in n and the existence of such an algorithm would disprove the commonly accepted conjecture $P \neq NP$, which is of vital importance in classical complexity theory.

The discovery of a polynomial-time algorithm would have enormous consequences: The (worst-case) performance of all known classical algorithms scales exponentially in the problem size n and already the solution of relatively small problems becomes classically impossible for all practical purposes. This is for example exploited in encryption protocols, see also section VI and section VIII in the appendix.

A. XYZ-Network

In order to find a good adiabatic quantum algorithm to reach the ground state of (25), we want to use the insight from the previous sections and try to construct an initial Hamiltonian H_I such that the interpolation from H_I to H_F corresponds to a phase transition of second or higher order. Since broken or restored symmetries are typically (though not always) associated with second-order phase transitions, we shall demand that H_I shares a symmetry with H_F and that this symmetry is broken in the initial ground state but restored in the final solution state. Furthermore, H_I should retain the interaction topology (i.e., bit structure) of H_F .

To this end, one can exploit the evident symmetry of the problem Hamiltonian (25) with respect to rotations around the axis generated by

$$\Sigma^z = \sum_{i=1}^n \sigma_i^z, \quad (26)$$

which we will further-on denote as Hamming-weight operator, since its eigenvalues are associated with the Hamming weight of the corresponding subspace. An obvious example for a Hamiltonian where this rotational symmetry is spontaneously broken is the $SO(3)$ -invariant ferromagnetic Hamiltonian

$$\begin{aligned} H_I^{xyz} &= - \sum_{i,j=1}^n |f_{ij}| \sigma_i \cdot \sigma_j \\ &= - \sum_{i,j=1}^n |f_{ij}| [\sigma_i^x \sigma_j^x + \sigma_i^y \sigma_j^y + \sigma_i^z \sigma_j^z], \end{aligned} \quad (27)$$

where we have used the same interaction topology f_{ij} as in (25). Clearly, this Hamiltonian is invariant under rotations around arbitrary axes – including (26) – whereas

its $(n + 1)$ -fold degenerate ground state singles out one specific direction, for example $|\uparrow\uparrow\dots\uparrow\rangle$.

This degeneracy immediately poses the question of which of these ground states should be used as the initial state. In analogy to the Ising model, where only the subspace with even bit-flip parity was relevant, this question can be answered by the conserved quantity (26). Since the final solution state will have a fixed Hamming weight Δ , we should start in the corresponding subspace $\mathcal{H}_\Delta = \{|\psi\rangle : \Sigma^z |\psi\rangle = \Delta |\psi\rangle\}$. Obviously, $|\uparrow\uparrow\dots\uparrow\rangle$ and $|\downarrow\downarrow\dots\downarrow\rangle$ correspond to $\Delta = n$ and $\Delta = -n$, respectively, and are not suitable (except in trivial cases). However, the state $|S\rangle = |\rightarrow\rightarrow\dots\rightarrow\rangle$ contains a superposition of all Hamming weights and can be used to project out an initial state with any desired value of $\Delta_k = 2k - n$ via

$$|\text{in}_k\rangle = \sqrt{\frac{2^n}{\binom{n}{k}}} \frac{1}{2n+1} \sum_{k=0}^{2n} \exp\left\{2\pi i \frac{\Delta_k - \Sigma_z}{2n+1} k\right\} |S\rangle \quad (28)$$

Up to normalization, above formula is just the Fourier decomposition of the Kronecker symbol $\delta(\Delta - \Sigma_z)$ and involves single-qubit rotations only. The state (28) can be prepared efficiently by different approaches such as for example projective measurements or adiabatic evolution [36]. Alternatively, one could use relaxation with an appropriate energy penalty in the Hamiltonian such as $(\Sigma^z - \Delta)^2$.

Of course, in order to prepare the initial state $|\text{in}\rangle$ correctly, one has to know the Hamming weight Δ of the solution bit-string – and in most adiabatic algorithms, this knowledge will not be available in advance. But since there are for an n -bit problem only $n + 1$ subspaces with different Hamming weights, a naive testing of all these possibilities corresponds to a polynomial overhead only. Moreover, for many problems such as *exact cover 3* discussed in the next section, one can guess the rough value of Δ and thereby limit the number of trials.

B. XY-Network

So far, we considered the fully $SO(3)$ rotationally symmetric ferromagnetic Hamiltonian (27). However, numerically we have found (at least for the *exact cover 3* problem) that the planar ferromagnetic model

$$H_I^{xy} = - \sum_{i,j=1}^n |f_{ij}| [\sigma_i^x \sigma_j^x + \sigma_i^y \sigma_j^y], \quad (29)$$

with the same interaction topology f_{ij} yields a better performance of the adiabatic algorithm (in average). In contrast to the spherically symmetric Hamiltonian (27), which is invariant under rotations around an arbitrary axis, this planar Hamiltonian is merely axially symmetric, i.e., invariant under rotations around the Σ^z -axis, i.e., $[H_I, \Sigma^z] = 0$.

Our conjecture is that for cases where the H_I^{xyz} initial Hamiltonian performs significantly worse, not only Σ^z is conserved exactly but – since this initial Hamiltonian commutes with $\mathbf{n} \cdot \Sigma = \mathbf{n} \cdot \sum_i \sigma_i$ – one might obtain additional nearly conserved quantities via $[\mathbf{n} \cdot \Sigma, H_F] \approx 0$. Since for an arbitrary vector \mathbf{n} , the final ground state may not have the symmetry, such nearly conserved quantities would strongly hamper the evolution from the initial ground state to the final one. Of course, the probability to find such an axis \mathbf{n} is greatly reduced for the H_I^{xy} initial Hamiltonians, which is consistent with our observation of increased performance.

Furthermore, the state $|S\rangle = |\rightarrow\rightarrow\dots\rightarrow\rangle$ (as well as arbitrary rotations of it around the Σ^z -axis) is no longer the *exact* ground state of (29) in general. These states are separable (no entanglement) whereas the true ground state of (29) is already entangled and cannot be given analytically for the general case. Fortunately, the mean-field approximation typically works reasonably well for a large number $n \gg 1$ of pseudo-randomly connected spins and hence the state $|S\rangle$ should provide a good *approximation* to the ground state. Indeed, numerically [37] we found that the state in (28) possesses a large overlap (over 90%) with the exact ground state (in the relevant subspace \mathcal{H}_Δ) and therefore provides a good initial state for the computation. Thus the exact $SO(3)$ degeneracy of the ground state in the xyz -network (27) is replaced by an approximate $O(2)$ degeneracy (mean-field approximation) in the xy -network (29). Nevertheless, both models imply a symmetry-restoring transition and thus should be of second order. Note that interestingly, neither (27) nor (29) are diagonal in the Hadamard basis, such that the arguments in [25] do not directly apply. In addition, these Hamiltonians differ strongly from projection operators (compare the discussion in [22, 23]).

V. EXACT COVER 3

A paradigmatic example for an NP-complete problem is *exact cover 3*: In this problem, one wants to find a bit-string $z_1 z_2 \dots z_{n-1} z_n$, where the n bits $z_\alpha \in \{0, 1\}$ must satisfy m constraints (clauses). For general 3-satisfiability (3-SAT), each of these clauses involves three bits $\alpha, \beta, \gamma \in \{1, \dots, n\}$ and for the specific *exact cover 3*-problem every clause is defined by the constraint

$$z_\alpha + z_\beta + z_\gamma = 1, \quad (30)$$

which has to be satisfied for every triple (α, β, γ) . A Hamiltonian encoding the solution to the *exact cover 3*-problem in its ground state can be defined by performing a sum over the (positive semidefinite) single-clause penalties (compare also [27, 34])

$$H_F = \sum_{c=1}^m (z_\alpha^c + z_\beta^c + z_\gamma^c - 1)^2. \quad (31)$$

Note that this problem Hamiltonian is slightly different from the original approach to *exact cover 3* [5], which

assigns a fixed energy penalty to each violated clause and thus involves three-qubit interactions [26], but has the same ground state (for satisfiable problems) – only some of the excitation energies differ. The above ansatz has the advantage that two-qubit operations suffice for its implementation, i.e., it is quadratic in the Pauli matrices. Inserting $z_i = \frac{1}{2}[\mathbf{1} - \sigma_i^z]$ one obtains

$$H_F = m\mathbf{1} - \sum_i \frac{n_i}{2} \sigma_i^z + \sum_{i,j} \frac{n_{ij}}{4} \sigma_i^z \sigma_j^z, \quad (32)$$

where $n_i > 0$ denotes the number of clauses involving the i^{th} bit and $n_{ij} \geq 0$ the number of clauses involving both bits i and j .

For *exact cover 3* our initial Hamiltonian (29) reads

$$H_I^{xy} = - \sum_{i,j=1}^n \frac{n_{ij}}{4} [\sigma_i^x \sigma_j^x + \sigma_i^y \sigma_j^y]. \quad (33)$$

Note that due to the relations $2n_i = \sum_j n_{ij}$ and $3m = \sum_i n_i$, the two-bit matrix n_{ij} of the final Hamiltonian defines an *exact cover 3*-problem completely.

In contrast, the original approach [5] employed the straight interpolation scheme with the initial Hamiltonian

$$H_I^{\text{conventional}} = \sum_i \frac{n_i}{2} [\mathbf{1} - \sigma_i^x], \quad (34)$$

which has the unique ground state (3) and no broken symmetry. In addition, it only contains the single-bit structure of the final Hamiltonian.

The Schrödinger equation is invariant under simultaneous transformations of time and energy, such that we need to compare the energy scales of our modified approach with the energy scales of the conventional ansatz [38]. The maximum energy spread of the quadratic final Hamiltonian (32) is $\Delta E_{\text{max}} = 4m$, which is only a factor of four larger than the conventional final Hamiltonian [5]. Likewise, the maximum energy of our initial Hamiltonian (33) can be upper bounded by $\Delta E_{\text{max}} \leq 6m$ (the same bound would apply for the XYZ-network), which is only a factor of two larger than $E_{\text{max}} = 3m$ for the conventional initial Hamiltonian (34). Therefore, the energy resources required by our modified algorithm are at most a factor of four larger than in the conventional approach.

Regarding the unknown Hamming weight of the solution, we found for *exact cover 3* that it is typically situated around $\Delta \approx n/3$, which drastically reduces the polynomial overhead generated by trying every possible value of Δ , see Sec. IV.

A. Hard exact cover 3 problems

In the following, we will numerically compare the effect of choosing the initial Hamiltonians (33) or (34) on the performance of adiabatic quantum computation. Of

course, this performance will depend on the selection of clauses in general. In order to select sufficiently hard problems, we only consider *exact cover 3* problems with just an unique satisfying agreement, as was also done in the original study [5]. However, there is evidence that this restriction is not sufficient yet for ensuring the highest computational complexity. For general 3-SAT, the number of instances with a unique satisfying agreement in combination with few clauses becomes exponentially rare among all instances with a unique satisfying agreement [24]. Also for *exact cover 3* random problem instances with a unique satisfying agreement include many simple sub-problems, which have to be sorted out in order to find hard instances [35]. Classically, the transition [39] from satisfiable to non-satisfiable problems for *exact cover 3* suggests that problems with rather few clauses ($m \approx 0.62n$) have the highest computational complexity.

In order to select problems near that classical phase transition in the small qubit range that is accessible to us, we have randomly generated two sets of 100 problem instances for each qubit number n : One problem set included only *exact cover 3* instances that have a unique satisfying solution and an arbitrary number of clauses (as considered in [5]). Another problem class did include *exact cover 3* instances with a unique solution and few clauses, specifically $m \leq \text{round}(2n/3)$. Note that this restriction explains the slight triple clustering of datapoints around qubit numbers divisible by 3 in figures 8, 10, 11, 12, and 13. Problem instances were generated similarly to [5] by successively adding random clauses until there was only one solution left. In the first problem set (analogous to [5]) the result was discarded (and the procedure started over) whenever the problem became unsatisfiable. In the second problem set we discarded the problem whenever either it became unsatisfiable or when the number of clauses exceeded the boundary $m \leq \text{round}(2n/3)$. Note that generating the latter problem set took a lot more effort than generating the first, which indicates that problems with a unique solution but few constraints are quite rare among all problems with a unique satisfying agreement – at least for the small qubit range accessible to us.

B. Adiabatic Runtime

Since analytic solutions are unfortunately not available, we have to compare the performance of the conventional approach (34) with our modified proposal (33) numerically. To this end, we first compute the adiabatic runtime T that is necessary to obtain a fixed final fidelity of $1/8$ for both schemes, see also [27]. In the conventional approach (34), the quantum state was initialized with the state $|S\rangle$ in (3), whereas it has been initialized with the normalized projection (28) of $|S\rangle$ onto the correct Hamming subspace in our scheme. For a range up to 20 qubits, the full Schrödinger equation had been integrated using a fourth order Runge-Kutta scheme [40] with an

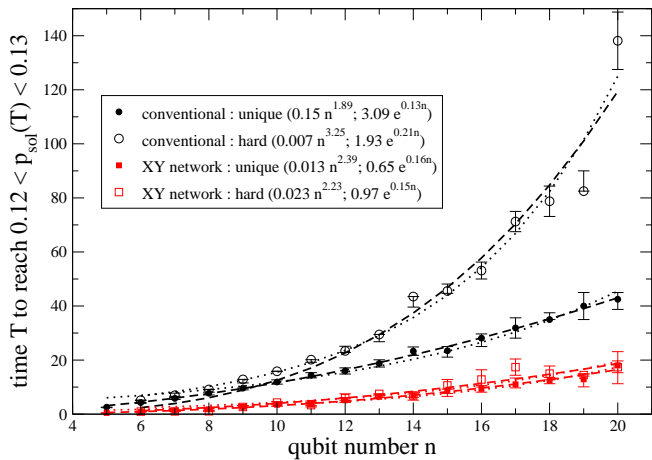


FIG. 8: [Color Online] Runtime necessary to yield a final ground state fidelity between 0.12 and 0.13. In all cases the new algorithm (orange) performed in average better than the conventional approach (black). Hollow symbols correspond to especially hard instances of the *exact cover 3* problem that do not only have a unique solution but also few clauses, in this case $m \leq \text{round}(2n/3)$. (This leads to a triple clustering of the hollow symbols around qubit numbers divisible by 3.) Dashed lines show polynomial fits, whereas dotted lines display exponential fits (values given in brackets).

adaptive step-size and varying run-times T , until an acceptable success probability in the final state was found, see figure 8. A considerably improved algorithmic performance was found – especially for the hard *exact cover 3* problems that have rather few clauses. For these hard problems, the conventional scheme performed in average significantly worse, whereas the new scheme did perform approximately similar on both problem classes.

However, it should be emphasized that the performance on a specific problem may deviate significantly from the average behavior: For example, we have also found some problems where the conventional scheme performed better than the new algorithm. The median plotted in figure 8 for reasons of visibility of error bars and compatibility with [5] is hardly sensitive to such rare instances. The worst case runtime we find (not shown) is not even a monotonously growing function of the number of qubits. For a given problem, it is therefore always practical to apply both quantum algorithms, since the solution can be tested in polynomial time.

C. Spectral Properties

In order to clarify the origin of the speed-up found for our scheme, we have also analyzed the lower part of the spectrum with the ARPACK package [37]: After determining the position of the critical point with a minimization algorithm [47] applied to $g(s) = E_1(s) - E_0(s)$, a parabola was fitted to $E_0(s)$ and to $E_1(s)$, see figure 9. Since determining the lower part of the spectrum at a

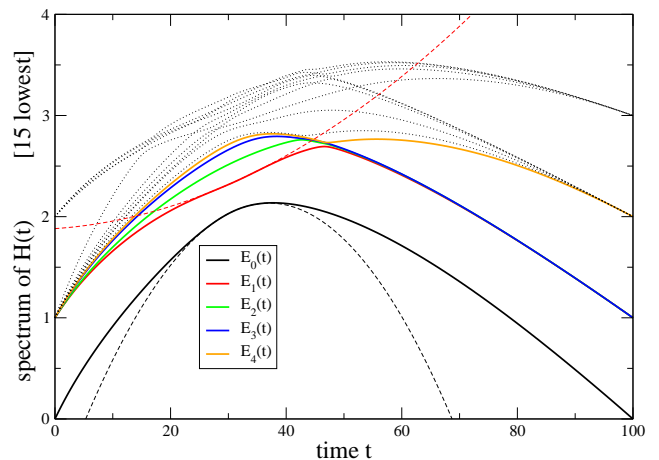


FIG. 9: [Color Online] Lower part of the spectrum for a typical *exact cover 3* instance with 10 qubits. After the position of the minimum gap was determined by a minimization algorithm, parabolae (dashed lines) were fitted to the lowest two eigenvalues.

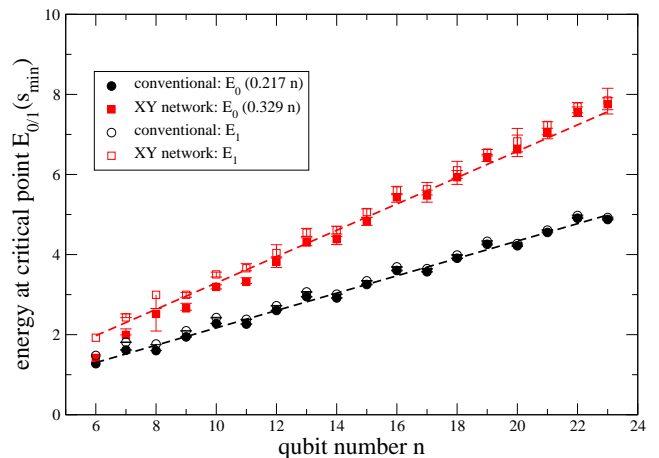


FIG. 10: [Color Online] Value of the energies of ground state (solid symbols) and the first excited state (hollow) at the position of the minimum gap for the conventional interpolation scheme (black) and the new approach (red) versus the number of qubits. Each symbol corresponds to the median of 100 random instances with a unique satisfying agreement and error bars give the 99% confidence interval on the median. Dashed lines display linear fits (fit parameters given in the legend in brackets) to the ground state energies and demonstrate that the modified algorithm has only a moderate increase in the ground state energy.

defined position is more efficient than integrating the full Schrödinger equation, we could extend our data range up to 23 qubits. In addition only the hard problem set with few clauses was considered here. The parameters of this parabola have been averaged over the 100 problem instances and are displayed in figures 10, 11, and 12, respectively. As one would expect, the scaling of the critical ground state energy is roughly linear for both algorithms, just the slope differs, see figure 10. It is also visible from

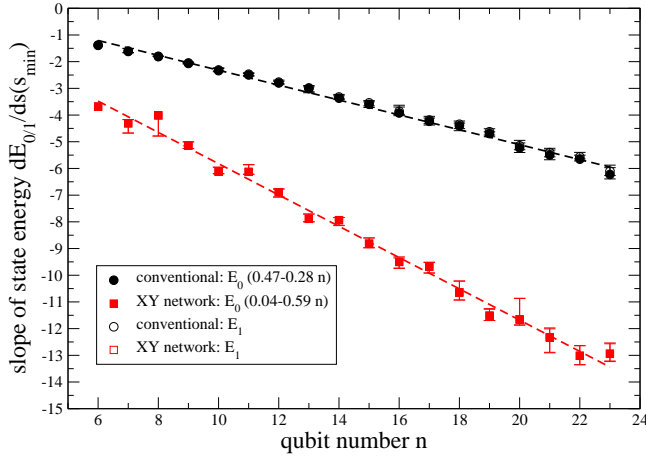


FIG. 11: [Color Online] Value of the derivative of the lowest two energies at the position of the minimum gap. Invisibility of the hollow symbols demonstrates that an extremal point of the fundamental gap has been found with high accuracy. Color coding and statistics are analogous to figure 10.

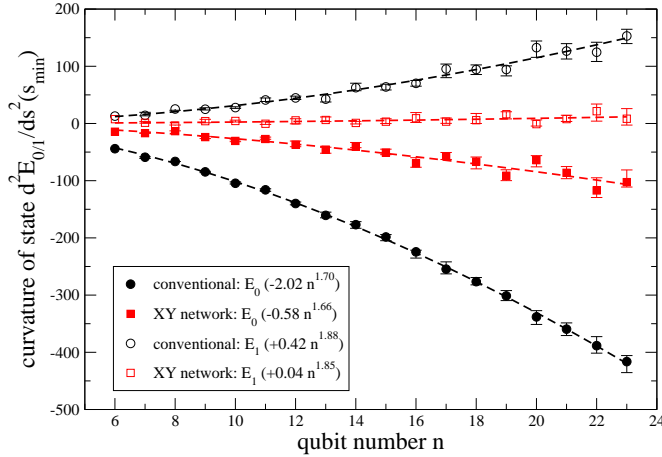


FIG. 12: [Color Online] Value of the curvature of the lowest two energies at the position of the minimum gap. Dashed lines represent polynomial fits (parameters shown in brackets). Color coding and statistics are analogous to figure 10.

figure 10 that the gap becomes smaller with increasing system size (as expected) and that the new approach has a larger minimum gap. The similar qualitative behavior holds also true for the average slope of the ground state energy at the critical point, see figure 11. However, for the curvature of the ground state energy – which is a direct marker for the order of the quantum phase transition, compare subsection II B – we obtain significant differences between the two algorithms. Whereas for the conventional algorithm the magnitude of the curvature of the ground state (and the first excited state) at the critical point increases strongly, for the new algorithm this scaling is drastically reduced – though still existent. This provides some evidence that by choosing the initial Hamiltonian of the form (33) with an approximately bro-

ken symmetry and retaining the two-bit structure of the final Hamiltonian one may indeed improve the order of the phase transition for *exact cover 3*.

D. Behavior of the fundamental gap

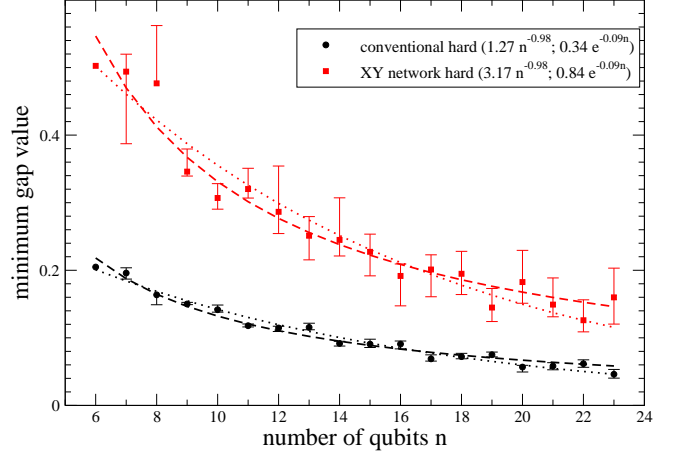


FIG. 13: [Color Online] Scaling of the value of the minimum gap versus the number of qubits. As one would expect, both scaling behaviors show a decrease with the system size. The vital question whether this scaling is polynomial (dashed fit lines) or exponential (dotted fit lines) cannot be answered with the limited numerical data. The minimum gap of our modified scheme is a factor of about 2.5 larger than in the conventional approach. Color coding and statistics are analogous to figure 10.

Although the absolute value of the minimum gap is larger in our new algorithm than in the conventional approach (see figure 13), the ratio of the two values does not seem entirely sufficient for explaining the strong differences in the adiabatic runtime in figure 8. Recalling the results of section III, we see that these results are compatible with the different behavior of the gap curvature, which can be deduced from figure 12 and is shown explicitly in figure 14. This is evidence that the adiabatic runtime can be positively influenced not only by the minimum fundamental gap alone but also by its curvature at the critical point. Note however that this is not too surprising, since for a smooth fundamental energy gap with a single minimum and that is bounded from below initially and finally, purely geometric arguments suggest that minimum gap and curvature at the minimum gap are related.

E. Entropy of Entanglement

Apart from the spectral properties of the Hamiltonian, entanglement is another very useful concept for the understanding of quantum phase transitions as well as quantum computing [3, 41]. If a quantum system is in

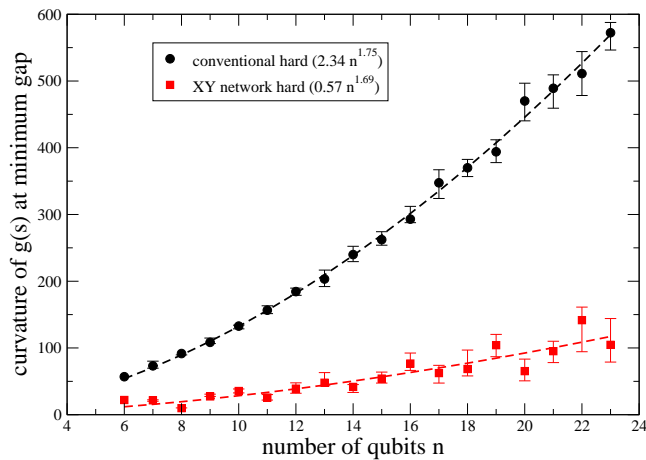


FIG. 14: [Color Online] Scaling of the fundamental gap curvature at the minimum gap versus the number of qubits. The curvature of our modified algorithm grows much slower as a function of n than with the conventional approach. Color coding and statistics are analogous to figure 10.

a pure state $\rho = |\Psi\rangle\langle\Psi|$, the entanglement between two subsystems can be quantified by the von-Neumann entropy

$$\begin{aligned} S_E &= S(\rho_1) = -\text{Tr}_1 \{ \rho_1 \log_2 \rho_1 \} \\ &= S(\rho_2) = -\text{Tr}_2 \{ \rho_2 \log_2 \rho_2 \}, \end{aligned} \quad (35)$$

of the reduced density matrix of either subsystem

$$\rho_1 = \text{Tr}_2 \{ \rho \}, \quad \rho_2 = \text{Tr}_1 \{ \rho \}, \quad (36)$$

where Tr_1 and Tr_2 denote the average over the degrees of freedom of subsystem 1 and 2, respectively. The quantity S_E is called entanglement entropy and has the property to vanish if and only if system and reservoir are not entangled, i.e., $S_E = 0 \Leftrightarrow |\Psi\rangle = |\Psi_1\rangle \otimes |\Psi_2\rangle$. It is also bounded by the smaller number of qubits in either subsystem $S_E \leq \min\{n_1, n_2\}$.

For general (sequential and adiabatic) quantum algorithms, it can be shown that an exponential speed-up is only possible if the entanglement S_E contained in the system (at some point of the calculation) grows sufficiently fast with system size [42]. On the other hand, a nonanalytic (e.g., diverging) behaviour of the entanglement S_E at the critical point (in the infinite size limit) is also a typical feature of quantum phase transitions. Let us illustrate these results by means of a few examples: The Ising model discussed in subsection II B (which is analytically solvable) displays a logarithmic scaling of the entanglement entropy near the critical point: The ground state entanglement entropy of a block of L spins scales mildly as $S_E \sim \ln L$, see e.g., [43] and references therein. In contrast to spin systems in higher spatial dimensions with a typical power-law scaling $S_E \sim n^p$, for example, this logarithmic growth rate would not be sufficient for an exponential speed-up. Shor's algorithm

contains order-finding [1], where the entanglement entropy between source and target register scales approximately linearly with the system size n [41]. The same scaling has been found (numerically) for adiabatic algorithms for *exact cover 3* by calculating the entanglement entropy for the first $n/2$ spins with the rest [41]. In comparison, the adiabatic Grover algorithm (with the same bipartition chosen) does also assume a maximum value of the entanglement entropy at the critical point – but this value remains constrained by one for all system sizes [41].

Here, we have numerically analyzed the behavior of the entanglement entropy of the instantaneous ground state. Imagining the n qubits as being lined up in a chain, we calculated the entanglement entropy between the subsystems formed by the first n_1 qubits and the remaining $n_2 = n - n_1$ qubits. Numerically, the entanglement entropy was found by calculating the instantaneous ground state $|\Psi_0(t)\rangle$ of the system [37] and then determining the reduced density matrix ρ_1 . Due to $S(\rho_1) = S(\rho_2)$ the largest reduced density matrices for $n = 10$ qubits have $N^2 = 32^2$ entries and can therefore be directly diagonalized [40]. The $n - 1$ values for the entanglement entropy resulting from the different partitions of an n -bit chain have simply been averaged. This resulting average was then again averaged over 100 (hard) problem instances of *exact cover 3*.

As one might have expected, the curves for the conventional scheme and our proposal differ strongly, see figure 15. For the conventional scheme, the entanglement entropy vanishes at the beginning and at the end of the calculation and possesses a pronounced peak at the critical point. In our algorithm, this peak is smeared out and we already start off with a relatively large entropy – the initial state in (28) is entangled, for a discussion of the required resources see subsection IV A. Moreover, the entropy is significantly larger in our algorithm throughout the interpolation. Both observations (i.e., the fact the entropy is larger and varies slower) could be interpreted as indications for the increased algorithmic performance – but one should bear in mind that the exact relation between the entanglement entropy and the achievable speed-up is not fully understood yet.

Increasing the number of qubits, we do also see the approximately linear scaling of the maximum entanglement entropy (in the qubit range that is accessible to us) observed in the literature [34].

VI. NUMBER FACTORIZATION

Apart from *exact cover 3*, there are many other problems whose solution can be encoded in the ground state of a quadratic Hamiltonian in (25). As one example, let us discuss the factoring problem (which is in NP, but not believed to be NP-complete), a further example is outlined in the appendix VIII.

Given a large number ω , it is in general very difficult to

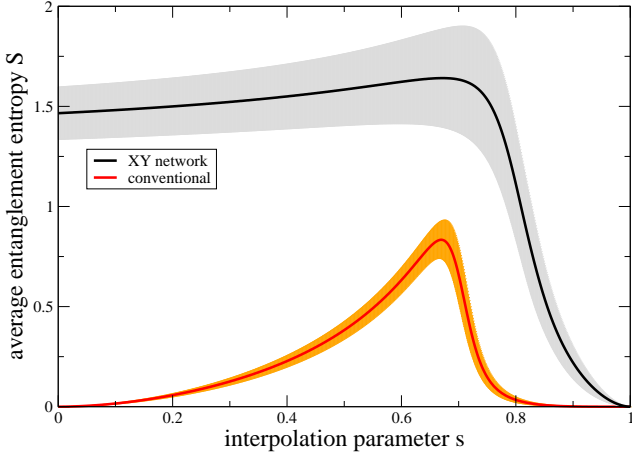


FIG. 15: [Color Online] Behavior of the average entanglement entropy for a system of 10 qubits. The shaded regions correspond to one standard deviation and the lines show the average over 100 problem instances.

answer the question which numbers a and b fulfill $\omega = ab$. The product of a k -bit number a and another $(n-k)$ -bit number b has either $(n-1)$ or n bits. In the following, we assume the latter case (the other option can be easily adapted by using $\omega_1 = 0$) and restrict our considerations to a Hilbert space with n qubits where the basis states can be written as $|\Psi\rangle = |a_1\rangle \dots |a_k\rangle |b_1\rangle \dots |b_{n-k}\rangle$. Of course, even for problems with a unique solution (e.g., biprimes with $k \neq n/2$), the partition $(k, n-k)$ will usually not be known in advance. However, the associated worst-case overhead of trying every possible value of k from $n/2$ to n grows only linearly as a function of n . A naive Hamiltonian encoding the solution as the ground state is then readily given by

$$H_{\text{F}}^{(1)} = (\omega - \hat{a}\hat{b})^2, \quad (37)$$

where

$$\begin{aligned} \hat{a} &= \sum_{\ell=1}^k \hat{a}_{\ell} 2^{k-\ell} &: \quad \hat{a}_{\ell} &= \frac{1}{2}(\mathbf{1} - \sigma_{\ell}^z), \\ \hat{b} &= \sum_{\ell=1}^{n-k} \hat{b}_{\ell} 2^{n-k-\ell} &: \quad \hat{b}_{\ell} &= \frac{1}{2}(\mathbf{1} - \sigma_{k+\ell}^z). \end{aligned} \quad (38)$$

Although it operates on a Hilbert space with dimension n and uses interactions between at most four qubits, the above Hamiltonian has the disadvantage that its couplings (operator pre-factors) cover an exponential range and thus its spectral range (ratio of largest and smallest eigenvalue) increases exponentially with the number of qubits n . In an experiment, an exponential fine-tuning of the couplings will probably be infeasible for the interesting case of large n . In addition, an exponentially increasing spectral width will be hard to realize without using exponential resources.

This scaling of the spectral width could be improved by

using the Hamming distance as a penalty in the Hamiltonian

$$H_{\text{F}}^{(2)} = \sum_{\ell=1}^n \left[\omega_{\ell} + (-1)^{\omega_{\ell}} (\hat{a}\hat{b})_{\ell} \right], \quad (39)$$

where ω_{ℓ} denotes the ℓ -th bit of ω , since here, the spectral width grows only linearly with the number of qubits. However, the computation of the ℓ -th bit of the product $\hat{a}\hat{b}$ requires simultaneous interactions of multiple qubits.

In the following, we construct a Hamiltonian that has at most two-qubit interactions and simultaneously a spectral width that scales only polynomially with the number of qubits. In addition, we demand that the local coupling constants should cover a finite range only.

A. Factorization Equations

To introduce our approach, let us consider as a generic example the case $n = 10$ and $k = 6$. Then, the usual method of multiplying two binary numbers can be decomposed into n equations according to Table I such as

$$\begin{aligned} a_1 b_4 + a_2 b_3 + a_3 b_2 + a_4 b_1 + z_{65} + z_{75} \\ - (\omega_5 + 2z_{54} + 4z_{53}) = 0, \end{aligned} \quad (40)$$

where the binary variables $z_{i>j}$ represent the carries from columns i towards j (the above equation corresponds to the fifth column). The complete set of equations like (40) are also called factorization equations, where a linear (plus logarithmic corrections) amount of carry variables z_{ij} is needed, see [44] for a detailed discussion. In an adiabatic quantum computer, these carry variables would have to be represented by additional qubits.

				a_1	a_2	a_3	a_4	a_5	a_6
				b_1	b_2	b_3	b_4		
				$a_1 b_4$	$a_2 b_4$	$a_3 b_4$	$a_4 b_4$	$a_5 b_4$	$a_6 b_4$
			$a_1 b_3$	$a_2 b_3$	$a_3 b_3$	$a_4 b_3$	$a_5 b_3$	$a_6 b_3$	
		$a_1 b_2$	$a_2 b_2$	$a_3 b_2$	$a_4 b_2$	$a_5 b_2$	$a_6 b_2$		
	$a_1 b_1$	$a_2 b_1$	$a_3 b_1$	$a_4 b_1$	$a_5 b_1$	$a_6 b_1$			
z_{21}	z_{32}	z_{43}	z_{54}	z_{65}	z_{76}	z_{87}	z_{98}		
z_{31}	z_{42}	z_{53}	z_{64}	z_{75}	z_{86}				
ω_1	ω_2	ω_3	ω_4	ω_5	ω_6	ω_7	ω_8	ω_9	ω_{10}

TABLE I: Conventional method for multiplying the $k = 6$ bit number a and the $n - k = 4$ bit number b . The result $\omega = ab$ is obtained by summing the partial products $a_i b_j$ and carry bits z_{ij} (from column i to column j), which gives rise to n factorization equations. Note that for this example, at most two carry bits are necessary in each column.

Obviously, factoring the number ω corresponds to finding a solution for the binary variables $(a_1, \dots, a_k, b_1, \dots, b_{n-k}, z_{ij})$ to the factoring equations. A simple idea is to assign a positive penalty to

each violated factoring equation *via*

$$H_F = \sum_{i=1}^n E_i^2, \quad (41)$$

where $E_i = 0$ expresses the i th factoring equation in normal form (with zero on the right hand side). Note however, that by naively using the square of the factorization equations we have generated four-qubit-interactions in the Hamiltonian. The maximum penalty originating from a single equation scales as $\mathcal{O}\{(n-k)^2\}$, such that the complete spectral width of this Hamiltonian scales in the worst case as $\mathcal{O}\{n^3\}$ (and so does the number of required four-qubit interactions). Although only a linear number of auxiliary qubits is needed, it may be experimentally difficult to realize so many different four-qubit interactions. In addition, our approach to generate higher-order phase transitions cannot be directly applied, since the Hamiltonian does not have the standard form of (25).

In order to obtain only two-qubit interactions, further modifications are necessary: Consider the case where only a single product of binary variables A and B is involved in each factoring equation

$$E = AB + S = 0, \quad (42)$$

where A and B are single bit variables and $S = \sum_j \alpha_j c_j$ is a sum of single bit variables with $\alpha_j \in \mathbb{Z}$. Then, the naive penalty for violating the equation (42), which would be given by $P_i = [AB + S]^2$, can be replaced by

$$\tilde{P}_E = 2 \left[\frac{1}{2} \left(A + B - \frac{1}{2} \right) + S \right]^2 - \frac{1}{8} \quad (43)$$

in the sense that both penalties vanish if and only if equation (42) is obeyed [which implies $(AB = 0 \wedge S = 0) \vee (AB = 1 \wedge S = -1)$] and are larger or equal to one otherwise. This modified penalty has the advantage that it involves only quadratic interactions between the qubits.

The task one is left with is to rewrite the multiplication table with the help of further ancilla variables such that only factorization equations of the type (42) occur. For the generic example, this is demonstrated in table II.

The general structure of the equations is for $1 \leq i \leq k$ and $1 \leq j \leq n-k$ is given by

$$a_i b_j + S_{ij} + z_{ij} = S_{i+1,j-1} + 2z_{i-1,j}, \quad (44)$$

where at the boundaries (marked by invalid indices) the equations are closed by

$$\begin{aligned} z_{0,j} &= S_{1,j-1}, \\ S_{i,0} &= \omega_i, \\ S_{k+1,j-1} &= \omega_{k+j}, \\ S_{i,n-k} &= z_{i,n-k} = 0, \\ z_{k,j} &= 0, \\ S_{1,n-k-1} &= 0. \end{aligned} \quad (45)$$

			a_1	a_2	a_3	a_4	a_5	a_6
			0	0	0	0	0	0
			$a_1 b_4$	$a_2 b_4$	$a_3 b_4$	$a_4 b_4$	$a_5 b_4$	$a_6 b_4$
			0	0	0	0	0	0
		0	S_{23}	S_{33}	S_{43}	S_{53}	S_{63}	
		$a_1 b_3$	$a_2 b_3$	$a_3 b_3$	$a_4 b_3$	$a_5 b_3$	$a_6 b_3$	
		z_{13}	z_{23}	z_{33}	z_{43}	z_{53}	0	
	S_{12}	S_{22}	S_{32}	S_{42}	S_{52}	S_{62}		
	$a_1 b_2$	$a_2 b_2$	$a_3 b_2$	$a_4 b_2$	$a_5 b_2$	$a_6 b_2$		
	z_{12}	z_{22}	z_{32}	z_{42}	z_{52}	0		
	S_{11}	S_{21}	S_{31}	S_{41}	S_{51}	S_{61}		
	$a_1 b_1$	$a_2 b_1$	$a_3 b_1$	$a_4 b_1$	$a_5 b_1$	$a_6 b_1$		
	z_{11}	z_{21}	z_{31}	z_{41}	z_{51}	0		
ω_1	ω_2	ω_3	ω_4	ω_5	ω_6	ω_7	ω_8	ω_9
								ω_{10}

TABLE II: Multiplication table for multiplying the 6 bit number a and the 4 bit number b using only two-qubit interactions. In each row, the first line contains the partial product sums, the second line the partial products, and the last line the carry variables. Note that the meaning of the indices for the auxiliary variables has changed in comparison to table I. Apart from the boundaries, the binary variables have to fulfill $a_i b_j + S_{ij} + z_{ij} = S_{i+1,j-1} + 2z_{i-1,j}$ (see the text for explanations). For each of the $(n-k-1=3)$ horizontal lines that have been inserted, $k=6$ partial product variables S_{ij} and $(k-1=5)$ carry variables z_{ij} have to be included. The first partial product variable (second row) always vanishes. Note also that the first partial product variable in each row is equal to the carry variable in the row above, which has therefore been removed.

With the suggested replacement in (43), this leads to the total penalty Hamiltonian

$$H_F^{(3)} = \sum_{i=1}^k \sum_{j=1}^{n-k} \left\{ 2 \left[\frac{1}{2} \left(\hat{a}_i + \hat{b}_j - \frac{1}{2} \right) + \hat{S}_{ij} + \hat{z}_{ij} - \hat{S}_{i+1,j-1} - 2\hat{z}_{i-1,j} \right]^2 - \frac{1}{8} \right\}, \quad (46)$$

where all operators act on distinct single qubits (for example on a two-dimensional lattice arrangement as $\hat{S}_{ij} = (\mathbf{1} - \sigma_{ij}^z)/2$). The above Hamiltonian has the ground state (an appropriate qubit ordering assumed)

$$|\Psi_g\rangle = |a_1 \dots a_k\rangle |b_1 \dots b_{n-k}\rangle |\{S_{ij}\}\rangle |\{z_{ij}\}\rangle, \quad (47)$$

where $\omega = ab$ is the sought-after factorization. The number of necessary auxiliary variables can be calculated as follows: In order to multiply a k -bit number a and a $(n-k)$ -bit number b , at most $k(n-k)$ partial products are required. For separating these into sums with a single product of two binary variables, $(n-k-1)$ horizontal lines have to be inserted, compare table II. Each of these lines requires k partial sum variables S_{ij} (except in the second row, where the first $S_{1,n-k-1}$ vanishes) and $(k-1)$ carry variables z_{ij} . Note that the bottom $(k-1)$

carry variables can be associated with the vanishing top $(k-1)$ carry variables. Therefore, the total number of auxiliary variables is given by $(2k-1)(n-k-1)-1$. Together with the n bits required for the factors a and b , at most $n-1+(2k-1)(n-k-1)$ qubits are required for finding the k and $n-k$ bit factors of an n -bit number. On an adiabatic quantum computer, this implies a quadratic overhead in the number of qubits. Since the number of variables in each factoring equation is always smaller or equal to 6, the total number of quadratic interactions scales with the number of equations, i. e., quadratically in n . For each equation in (46), the largest possible penalty is 21, which leads to a quadratical scaling of the spectral width. Note also that the necessary coupling strength between different qubits ranges (independent of the problem size) from 1 to 8.

B. Numerical Study

Similar to satisfiability problems – where those with a unique solution are believed to belong to the hardest problems [5] (both classically and in adiabatic quantum algorithms), bi-primes (products of two prime numbers) possess a unique factorization and the classical hardness of bi-prime factorization is used in many cryptography protocols. Except in the case $k = n/2$ (where the solution becomes two-fold degenerate due to $\omega = ab = ba$), the Hamiltonians have a unique ground state. In our case, biprime factorization constitutes a well-defined (and also classically relevant) problem class, for which the algorithmic performance of an adiabatic quantum algorithm using (46) as the problem Hamiltonian would be interesting.

In order to reduce the problem complexity of (46), one can use the fact that both prime factors are odd in non-trivial cases and that there exists a minimum size of the prime factors to generate an n -bit number, i.e., that both first and last bits of the prime factors are set to 1, see table III for the generic example. Under these conditions, the first row generates $k-1$ nontrivial equations that involve no product between different qubits at all. In these, the S_{ij} variables can be eliminated without changing the structure of the equations. Together with the $(n-4)$ bits required to store the unknown bits of the prime factors, one arrives at $[2k(n-k-1)-3]$ variables to find the odd $(k, n-k)$ factors of the n -bit number ω . Finally, the two-qubit Hamiltonian can be cast into the form

$$H_F = h + \sum_{i=1}^{n_{\text{tot}}} h_i \sigma_i^z + 2 \sum_{i=1}^{n_{\text{tot}}} \sum_{j=i+1}^{n_{\text{tot}}} h_{ij} \sigma_i^z \sigma_j^z, \quad (48)$$

where n_{tot} denotes the total number of qubits and $h, h_i, h_{ij} \in \mathbb{R}$ with $h_{ij} = h_{ji}$ and $h_{ii} = 0$. It is easy to see that the coefficients h, h_i, h_{ij} can be conveniently extracted from eqn. (46) by computing traces of $H_F^{(3)}$, $\sigma_i^z H_F^{(3)}$, and $\sigma_i^z \sigma_j^z H_F^{(3)}$, respectively. We have analyzed

the algorithmic performance for a linear interpolation for three different initial Hamiltonians

$$\begin{aligned} H_I^x &= \sum_{i=1}^{n_{\text{tot}}} \frac{1}{2} [\mathbf{1} - \sigma_i^x], \\ H_I^{xy} &= \sum_{i,j=1}^{n_{\text{tot}}} \frac{|h_{ij}|}{4} [\mathbf{2} - \sigma_i^x \sigma_j^x - \sigma_i^y \sigma_j^y], \\ H_I^{xyz} &= \sum_{i,j=1}^{n_{\text{tot}}} \frac{|h_{ij}|}{4} [\mathbf{1} - \sigma_i^x \sigma_j^x - \sigma_i^y \sigma_j^y - \sigma_i^z \sigma_j^z]. \end{aligned} \quad (49)$$

Note that the first Hamiltonian has the ground state $|S\rangle$ in (3) and no apparent symmetry of the final Hamiltonian is respected. The latter two Hamiltonians commute with the Hamming-weight operator (26) and the same discussion as in section V applies. However, there are also some crucial differences:

- In contrast to *exact cover 3*, the numbers h_{ij} in the quadratic decomposition (48) are not necessarily positive.
- In addition, unlike *exact cover 3*, the two-bit interactions h_{ij} do not completely determine the problem, such that the Hamiltonians in (49) can probably be further improved.

			1	a_2	a_3	a_4	a_5	1
		0	1	a_2	a_3	a_4	a_5	1
		b_3	$a_2 b_3$	$a_3 b_3$	$a_4 b_3$	$a_5 b_3$	b_3	
		z_{13}	z_{23}	z_{33}	z_{43}	z_{53}	0	
	S_{12}	S_{22}	S_{32}	S_{42}	S_{52}	S_{62}		
	b_2	$a_2 b_2$	$a_3 b_2$	$a_4 b_2$	$a_5 b_2$	b_2		
	z_{12}	z_{22}	z_{32}	z_{42}	z_{52}	0		
	S_{11}	S_{21}	S_{31}	S_{41}	S_{51}	S_{61}		
	1	a_2	a_3	a_4	a_5	1		
	z_{11}	z_{21}	z_{31}	z_{41}	z_{51}	0		
ω_1	ω_2	ω_3	ω_4	ω_5	ω_6	ω_7	ω_8	ω_9
								1

TABLE III: Multiplication table for multiplying the odd 6 bit number a and the odd 4 bit number b . The $(k-1)$ S_{ij} -variables in the top row of table II have been eliminated without changing the structure of the equations. One equation (top right) becomes trivial, whereas (from top to bottom) $k-1+2(n-k-2)+k=2n-5$ equations emerge that involve no products between different qubits at all.

Since we can with moderate effort simulate the evolution of systems with $\mathcal{O}(20)$ qubits, we can numerically access the $(n, n-k)$ factoring partitions displayed in table IV. For the bi-primes within this range, we have determined the minimum fundamental gap during the linear interpolation [37], see figure 16. It is visible that again the H_I^{xy} Hamiltonian is superior to the other choices in (49) – at least for the small sample problems under consideration.

Interestingly, the third Hamiltonian in (49) leads in some cases to an even smaller minimum gap than with the conventional choice. We have also observed this for rare instances of EC3. As discussed in subsection IV B, we conjecture additional nearly conserved quantities to hamper the adiabatic evolution towards the solution in case of the H_1^{xyz} initial Hamiltonian.

n_{tot}	bi-primes	partitions ($n, n - k$)
5	33;39	(4,2);(4,2)
7	51;57;69;87;93	(5,2);(5,2);(5,2);(5,2);(5,2)
9	25;35;49;111;123	(3,3);(3,3);(3,3);(6,2);(6,2)
	129;141;159;177;183	(6,2);(6,2);(6,2);(6,2);(6,2)
13	55;65;77;91	(4,3);(4,3);(4,3);(4,3)
17	85;95;115;119;133	(5,3);(5,3);(5,3);(5,3);(5,3)
	145;155;161;203;217	(5,3);(5,3);(5,3);(5,3);(5,3)
21	121;143;169	(4,4);(4,4);(4,4)

TABLE IV: Bi-primes and partitions accessible with different numbers of qubits (leftmost column).

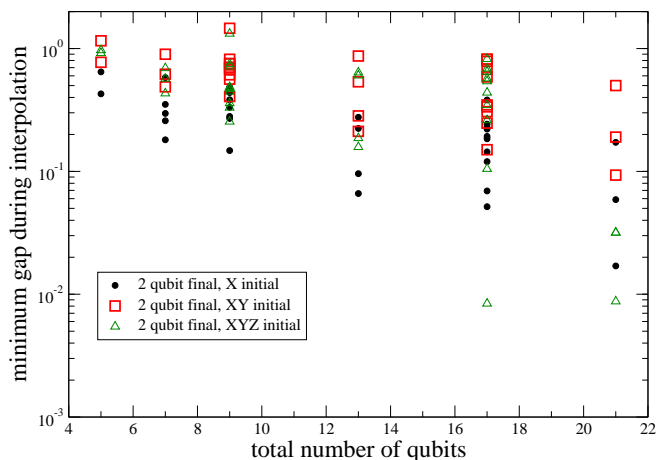


FIG. 16: [Color Online] Minimum gap during adiabatic interpolation for number factorization versus the total number of qubits used. For problems with a doubly degenerate ground state, the minimum gap between the lowest and the second excited state has been calculated. Each data set has the same number of data points per column (some symbols lie on top of each other).

VII. CONCLUSIONS

In summary, the analogy between adiabatic quantum algorithms and quantum phase transitions yields new insight and facilitates a better understanding of both. For first-order transitions, the system has to tunnel through an energy barrier in order to stay in the ground state (cf. Fig. 2), which indicates an exponential scaling of the tunneling time with system size. Since such a tunneling barrier is absent for transition of second or higher order

(cf. Fig. 4), we conjecture that they are advantageous with respect to adiabatic quantum computation in the sense that they allow much shorter run-times.

Based on this physical intuition, we designed a modified adiabatic quantum algorithm for the NP-complete problem *exact cover 3* in analogy to a symmetry-restoring quantum phase transition and found numerically that it indeed yields an improved performance in comparison with the conventional scheme. Even though the infinite-size limit of these adiabatic quantum algorithm may not be as well-defined as that of the Ising model (probably they should be classified somewhere between first and second order), the spectral characteristics indicate that our alternative adiabatic quantum algorithm has a higher order than the conventional scheme.

As a closely related point, we observed that the adiabatic run-time (of constant-speed interpolations) is not just determined by the value of the minimum gap but also by the curvature of the energy levels at the critical point. In fact, the better average scaling behavior of our alternative algorithm can probably be attributed mostly to the fact that the energy levels are far less curved than in the conventional scheme.

Apart from the spectral characteristics, entanglement is another useful concept for quantum algorithms as well as quantum phase transitions. We found that the ground-state entanglement entropy in our modified adiabatic quantum algorithm is much larger than that in the conventional scheme, which might be connected with the advantages of higher-order phase transitions. However, these advantages may also go along with some drawbacks: for the prototypical Grover and Ising models, we found that second-order phase transitions seem to be more vulnerable to decoherence than those of first order [17, 18].

Finally, even though the run-time scaling (polynomial versus exponential) is not clear, the results obtained so far strongly suggest that adiabatic quantum algorithm can solve NP problems much faster than the Grover search routine (with a quadratic speed-up). The methods proposed in this article can easily be applied to other computationally relevant problems which can be encoded into the ground states of Hamiltonians that are quadratic in the Pauli matrices – such as factoring (see also the Appendix VIII).

Acknowledgements

This work was partly supported by the Emmy Noether Programme of the German Research Foundation (DFG) under grant No. SCHU 1557/1-2. R. S. acknowledges fruitful discussions at the Les Houches Summer School on Quantum Magnetism and the Banff (BIRS) workshop on “Spin, Charge, and Topology” (supported by PITP), and valuable conversations with G. Volovik (visits supported by EU-ULTI and ESF-COSLAB). The authors are indebted to F. Krauss for providing computational resources and to E. Farhi, J. Goldstone, and R. Plaga for

fruitful discussions.

* schaller@itp.physik.tu-berlin.de

† schuetz@theo.physik.uni-due.de

VIII. APPENDIX: ENCRYPTION WITH TEA

Although factoring numbers is also used in encryption algorithms, it is by no means the only way to encode or decode information. One further example is the *Tiny Encryption Algorithm* (TEA). The C-code for TEA [45] is publically available and the algorithm has not been broken – i.e., there is no known classical algorithm which finds the key significantly faster (with input and output given) than the simple brute-force search. In its standard form, it encodes 64 input bits using a 128 bit key. Encoding is done by an iterative procedure that performs – depending on the values of the key bits – different operations on the input bits. With knowledge of the key, these operations are easily invertible, whereas without the key the inversion of the encryption becomes exponentially complex. Therefore, extracting the key from a given input and its encrypted output would open a way to decode all information that has been encrypted with this key.

Here we will demonstrate that in principle it is possible – if input and output are known (e.g., for a specific communication) – to encode the search for the key in the ground state of a quadratic Hamiltonian of the form (25). With the input given by the $n = 32$ bit numbers y^1 and z^1 and the output by the 32-bit numbers y^ℓ and z^ℓ , the TEA algorithm establishes a relation between these and the encryption key numbers k_a, k_b, k_c, k_d by forming the sequence

$$\begin{aligned} y^{i+1} &= [S_4^-(z^i) + k_a] \oplus [z^i + s^i] \oplus [S_5^+(z^i) + k_b], \\ z^{i+1} &= [S_4^-(y^i) + k_c] \oplus [y^i + s^i] \oplus [S_5^+(y^i) + k_d], \end{aligned}$$

where the index i runs from 1 to $\ell - 1$. Here \oplus denotes bitwise addition (XOR), S_a^\pm defines left- and right-bit-shifting by a digits, and s^i are some fixed (known) numbers given by the algorithm. In its standard form, the algorithm uses $\ell = 32$ iterations. Obviously, in each of the three different operations used – adding of two numbers, bit shifting and bitwise addition (XOR) – always one of the two operands is defined by the key or by the encryption algorithm. Therefore, knowledge of input, output and the key enables one to reverse the process (of course, with knowledge of the encryption algorithm assumed). From the previous section it is evident that the addition of two n -bit numbers [none of which is known – e.g., $S_4^-(z^i) + k_a$] can be encoded in the ground state of a quadratic Hamiltonian using just n ancilla bits. Using the replacement (43), the same is possible for the XOR operation. Note that the bit shifting used does not pose any (theoretical) problem, since it just changes the index of qubits which have to interact. In each iteration of (50) one has 4 XOR operations and 4 non-trivial additions (where both addends are unknown). Therefore, a quadratic Hamiltonian would not only operate on the key bits k_a, k_b, k_c, k_d but also on the intermediate results y^i, z^i as well as the ancilla qubits. In each iteration, $\mathcal{O}\{n\}$ auxiliary qubits are required, such that an overall number of $\mathcal{O}\{n\ell\}$ bits will suffice to encode the search for the key in the ground state of a quadratic Hamiltonian. *Ergo*, similar to factoring, we obtain a quadratic overhead and thus one might expect that an adiabatic quantum algorithm might find the key much faster than the Grover (brute-force) search.

-
- [1] P. W. Shor, SIAM J. Comp. **26**, 1484 (1997).
 [2] L. K. Grover, Phys. Rev. Lett. **79**, 325 (1997).
 [3] M. A. Nielsen and I. L. Chuang, *Quantum Computation and Quantum Information*, Cambridge University Press, Cambridge (2000).
 [4] P. Aliferis, D. Gottesman, and J. Preskill, Quant. Inf. Comp. **6**, 97-165 (2006).
 [5] E. Farhi *et al.*, Science **292**, 472 (2001).
 [6] E. Farhi *et al.*, e-print: quant-ph/0001106 (2001).
 [7] D. Aharonov *et al.*, 45th Annual IEEE Symposium on Foundations of Computer Science, 42-51 (2004); e-print: quant-ph/0405098.
 [8] M. S. Sarandy, L.-A. Wu and D. A. Lidar, Quant. Inform. Proc. **3**, 331 (2004).
 [9] A. M. Childs, E. Farhi, and J. Preskill, Phys. Rev. A **65**, 012322 (2001).
 [10] M. S. Sarandy and D. A. Lidar, Phys. Rev. A **71**, 012331 (2005).
 [11] M. S. Sarandy and D. A. Lidar, Phys. Rev. Lett. **95**, 250503 (2005).
 [12] J. Roland and N. J. Cerf, Phys. Rev. A **71**, 032330 (2005).
 [13] J. Åberg, D. Kult, and E. Sjöqvist, Phys. Rev. A **71**, 060312(R) (2005).
 [14] J. Åberg, D. Kult, and E. Sjöqvist, Phys. Rev. A **72**, 042317 (2005).
 [15] P. Thunström, J. Åberg, and E. Sjöqvist, Phys. Rev. A **72**, 022328 (2005).
 [16] N. Shenvi, K. R. Brown, and K. B. Whaley, Phys. Rev. A **68**, 052313 (2003).
 [17] M. Tiersch and R. Schützhold, Phys. Rev. A **75**, 062313 (2007).
 [18] S. Mostame, G. Schaller, and R. Schützhold, Phys. Rev. A **76**, 030304(R) (2007).
 [19] G. Schaller, S. Mostame, and R. Schützhold, Phys. Rev. A **73**, 062307 (2006).
 [20] S. Jansen, M. B. Ruskai, and R. Seiler, J. Math. Phys. **48**, 102111 (2007).
 [21] J. Roland and N. J. Cerf, Phys. Rev. **65**, 042308 (2002).

- [22] M. Žnidarič and M. Horvat, Phys. Rev. A **73**, 022329 (2006).
- [23] E. Farhi *et al.*, Int. J. Quant. Inf. **6**, 503-516 (2008).
- [24] M. Žnidarič, Phys. Rev. A **71**, 062305 (2005).
- [25] L. M. Ioannou and M. Mosca, Int. J. Quant. Inf. **6**, 419 - 426 (2008).
- [26] J. I. Latorre and R. Orus, Phys. Rev. A **69**, 062302 (2004).
- [27] R. Schützhold and G. Schaller, Phys. Rev. A **74**, 060304(R) (2006).
- [28] E. Farhi, J. Goldstone, and S. Gutmann, e-print:quant-ph/0201031 (2002).
- [29] E. Farhi, J. Goldstone, and S. Gutmann, e-print:quant-ph/0208135 (2002).
- [30] S. Sachdev, *Quantum Phase Transitions*, Cambridge University Press, Cambridge (2000).
- [31] J. Dziarmaga, Phys. Rev. Lett. **95**, 245701 (2005).
- [32] G. Schaller, Phys. Rev. A **78**, 032328 (2008).
- [33] R. Schützhold, J. Low Temp. Phys. **153**, 228 (2008).
- [34] M. C. Banuls *et al.*, Phys. Rev. A **73**, 022344 (2006).
- [35] A. P. Young, S. Knysh and V. N. Smelyanskiy, Phys. Rev. Lett. **101**, 170503 (2008).
- [36] A. M. Childs *et al.*, Quant. Inf. Comp. **2**, 181 (2002).
- [37] R. B. Lehoucq, D. C. Sorensen, and C. Yang, *ARPACK Users' Guide: Solution of Large-Scale Eigenvalue Problems with Implicitly Restarted Arnoldi Methods*, SIAM (1998); see also <http://www.caam.rice.edu/software/ARPACK>.
- [38] S. Das, R. Kobes, and G. Kunstatter, J. Phys. A **36**, 2839-2845, (2003).
- [39] V. Kalapala and C. Moore, e-print: cs.CC/0508037 (2005).
- [40] W. H. Press *et al.*, *Numerical Recipes in C*, Cambridge University Press, Cambridge (1994).
- [41] R. Orus and J. I. Latorre, Phys. Rev. A **69**, 052308 (2004).
- [42] G. Vidal, Phys. Rev. Lett. **91**, 147902 (2003).
- [43] L. Cincio *et al.*, Phys. Rev. A **75**, 052321 (2007).
- [44] C. J. C. Burges, *Factoring as Optimization*, Microsoft Research MSR-TR-2002-83, Technical Report (2002).
- [45] D. J. Wheeler and R. M. Needham, Lecture Notes in Computer Science **1008**, 363-366 (1994); see also <http://www.simonshpherd.supanet.com/tea.htm>.
- [46] From the classical point of view, finding the ground state of (25) corresponds to finding the n -bit bit-string $z_1 \dots z_n$ for which $E = \sum_{i=1}^n f_i(1 - 2z_i) + \sum_{i,j} f_{ij}(1 - 2z_i)(1 - 2z_j)$ has the minimum value. The quadratic form f_{ij} can always be made positive definite without changing its value on the binary numbers by adding terms of the form $z_i^2 - z_i$. Although the minimum of a positive definite quadratic form in n dimensions can easily be found in the set of real numbers with a standard minimization algorithm, it must be kept in mind that the above-posed problem implies the side constraints that the numbers have to be binaries. These side constraints have to be expressed by higher-order polynomials [such as e.g., $\sum_i x_i^2(1 - x_i)^2$], which lead to the existence of many local minima and classical minimization algorithms will have difficulties to find the global minimum.
- [47] Of course, for the determination of the eigen-energies of the new approach we did only consider the relevant Hamming subspace.